Grid-based diffusion Monte Carlo for fermions without the fixed-node approximation

Alexander A. Kunitsa [*] and So Hirata

Department of Chemistry, University of Illinois at Urbana-Champaign, Urbana, Illinois 61801, USA

A diffusion Monte Carlo algorithm is introduced that can determine the correct nodal structure of the wave function of a few-fermion system and its ground-state energy without an uncontrolled bias. This is achieved by confining signed random walkers to the points of a uniform infinite spatial grid, allowing them to meet and annihilate one another to establish the nodal structure without the fixed-node approximation. An imaginary-time propagator is derived rigorously from a discretized Hamiltonian, governing a non-Gaussian, sign-flipping, branching, and mutually annihilating random walk of particles. The accuracy of the resulting stochastic representations of a fermion wave function is limited only by the grid and imaginary-time resolutions and can be improved in a controlled manner. The method is tested for a series of model problems including fermions in a harmonic trap as well as the He atom in its singlet or triplet ground state. For the latter case, the energies approach from above with increasing grid resolution and converge within $0.015\,E_h$ of the exact basis-set-limit value for the grid spacing of 0.08 a.u. with a statistical uncertainty of $10^{-5}\,E_h$ without an importance sampling or Jastrow factor.

I. INTRODUCTION

Stochastic algorithms [1–3] hold exceptional promise in treating correlated electronic structures owing to their high parallel efficiency, near-exact accuracy, scalability with the problem size, and tiny memory footprints. Perhaps, the most successful of such algorithms is diffusion Monte Carlo (DMC) [2], but it is notoriously plagued by an uncontrolled bias (the fixed-node error) arising from the fixed-node approximation [2,4,5] introduced as a practical solution to the sign problem [6]. It amounts to using the nodal structure of some trial wave function, which differs from the exact one, thus causing the error.

The objective of this work is to eliminate the fixed-node error from DMC [2]. This is achieved by confining the positively and negatively signed walkers on an infinite, uniform, real-space grid, which can thus meet on a grid point and then annihilate one another, establishing a nodal structure without the fixed node or any other similar approximation. The resulting nodal structure should converge at the exact one in the limit of infinitesimally small grid spacing and imaginary time step. A general stochastic propagation protocol on a grid is derived in this work. Our method—grid DMC—is distinguished from any of the previously developed fermion quantum Monte Carlo approaches that enforce annihilation by walker pairing, correlated dynamics, or other techniques [7–13].

Casula *et al.* [14,15] were among the first to introduce a real-space grid in DMC but for the different purpose of implementing a nonlocal pseudopotential. Like their method, our grid DMC relies on a finite-difference approximation to the kinetic-energy operator on a grid. It also shares some

algorithmic features with full configuration interaction quantum Monte Carlo (FCIQMC), which propagates signed walkers in a discretized space of the Slater determinants, the latter ensuring the fermion antisymmetry of the wave function [16]. Grid DMC obeys a similar population dynamics as FCIQMC, which is an interplay between propagation, branching, and annihilation of walkers [17]. A correct nodal structure emerges as the total number of walkers exceeds a critical value, N_c, which is a function of the grid spacing, dimension of the configuration space, and character of the target state. The value of N_c determines the memory footprint, which is expected to grow exponentially with the system size as a manifestation of the sign problem [6].

Clearly, grid DMC is severely limited in its applicability because of the exponential size dependence of N_c if one insists on solving the Schrödinger equation essentially exactly. In this work, we establish its feasibility just for two-particle (Coulomb) systems in the three-dimensional (3D) space with a view to ultimately realizing DMC-like stochastic algorithms for two-electron theories such as second-order Møller-Plesset perturbation (MP2) [18–21] or coupled-cluster doubles (CCD) theory [22] in real space. Stochastic MP2 and CCD may be expected to be more scalable than their deterministic counterparts (with respect to both the number of processors and problem size) and thus applicable to large systems that do not lend themselves to local-correlation speedup.

This article is structured as follows: A detailed description of our grid DMC algorithm is given in Sec. II. The results of demonstrative calculations on fermions in a harmonic trap and the He atom in the triplet or singlet ground state are reported in Secs. III A and III B, respectively. A summary of the method and an outline of the future work are given in Sec. IV. In Appendices A and B, mathematical details of the algorithm are given.

---

[*]aakunitsa@gmail.com

013311-1

II. THEORY AND ALGORITHMS

Let $\Psi(\boldsymbol{r}_1, \ldots, \boldsymbol{r}_N, \tau)$ be the wave function of an N-particle system satisfying the imaginary-time-dependent Schrödinger equation with energy offset ω,

$$-\frac{\partial \Psi(\boldsymbol{r}_1, \ldots, \boldsymbol{r}_N, \tau)}{\partial \tau} = (\hat{H} - \omega)\Psi(\boldsymbol{r}_1, \ldots, \boldsymbol{r}_N, \tau), \quad (1)$$

where $\hat{H}$ is the Hamiltonian with a local, spin-independent potential $V(\boldsymbol{r}_1, \ldots, \boldsymbol{r}_N)$,

$$\hat{H} = -\frac{1}{2}\sum_{i=1}^{N} \nabla_i^2 + V(\boldsymbol{r}_1, \ldots, \boldsymbol{r}_N). \quad (2)$$

Equation (1) suggests that, starting from an arbitrary initial wave function $\Phi(\boldsymbol{r}_1, \ldots, \boldsymbol{r}_N)$, one can reach the exact ground-state wave function $\Psi(\boldsymbol{r}_1, \ldots, \boldsymbol{r}_N)$ by

$$\Psi(\boldsymbol{r}_1', \ldots, \boldsymbol{r}_N', \tau) = \int d\{\boldsymbol{r}_i\} G(\boldsymbol{r}_1, \ldots, \boldsymbol{r}_N$$
$$\rightarrow \boldsymbol{r}_1', \ldots, \boldsymbol{r}_N'; \tau)\Phi(\boldsymbol{r}_1, \ldots, \boldsymbol{r}_N), \quad (3)$$

insofar as $\Phi(\boldsymbol{r}_1, \ldots, \boldsymbol{r}_N)$ is not orthogonal to $\Psi(\boldsymbol{r}_1, \ldots, \boldsymbol{r}_N)$ and ω is chosen to be equal to the exact ground-state energy. $G(\boldsymbol{r}_1, \ldots, \boldsymbol{r}_N \rightarrow \boldsymbol{r}_1', \ldots, \boldsymbol{r}_N'; \tau)$ is the imaginary-time Green's function or propagator written as

$$G(\boldsymbol{r}_1, \ldots, \boldsymbol{r}_N \rightarrow \boldsymbol{r}_1', \ldots, \boldsymbol{r}_N'; \tau)$$
$$= \langle \boldsymbol{r}_1', \ldots, \boldsymbol{r}_N'| \exp[-\tau(\hat{H} - \omega)]|\boldsymbol{r}_1, \ldots, \boldsymbol{r}_N\rangle, \quad (4)$$

where $|\boldsymbol{r}_1, \ldots, \boldsymbol{r}_N\rangle$ is a position eigenfunction.

In DMC [2,3], the imaginary-time propagation [Eq. (3)] is interpreted as a branching random walk of the fictitious particles in $3N$-dimensional space. The transition probability of the particles hopping from $(\boldsymbol{r}_1, \ldots, \boldsymbol{r}_N)$ to $(\boldsymbol{r}_1', \ldots, \boldsymbol{r}_N')$ in short time τ is approximated using the Suzuki-Trotter expansion of the Green's function [23]:

$$G(\boldsymbol{r}_1, \ldots, \boldsymbol{r}_N \rightarrow \boldsymbol{r}_1', \ldots, \boldsymbol{r}_N'; \tau)$$
$$\approx \langle \boldsymbol{r}_1', \ldots, \boldsymbol{r}_N'| \exp\{-\tau(V - \omega)/2\}|\boldsymbol{r}_1', \ldots, \boldsymbol{r}_N'\rangle$$
$$\times \langle \boldsymbol{r}_1', \ldots, \boldsymbol{r}_N'| \exp\left(\tau \sum_{i=1}^{N} \nabla_i^2/2\right)|\boldsymbol{r}_1, \ldots, \boldsymbol{r}_N\rangle$$
$$\times \langle \boldsymbol{r}_1, \ldots, \boldsymbol{r}_N| \exp\{-\tau(V - \omega)/2\}|\boldsymbol{r}_1, \ldots, \boldsymbol{r}_N\rangle \quad (5)$$

$$= \exp\left\{-\tau\left(\frac{V(\{\boldsymbol{r}_i'\}) + V(\{\boldsymbol{r}_i\})}{2} - \omega\right)\right\} \prod_{i=1}^{N} \langle \boldsymbol{r}_i'| \exp\left(\tau \nabla_i^2/2\right)|\boldsymbol{r}_i\rangle, \quad (6)$$

where the use has been made of the fact that $|\boldsymbol{r}_1, \ldots, \boldsymbol{r}_N\rangle$ is an eigenfunction of $\exp\{-\tau(V - \omega)/2\}$.

In this work, a particle is confined to a point in an infinite, uniform, 3D grid with grid spacing δ. The Laplacian in the kinetic-energy operator is approximated by a central three-point finite-difference formula. In this ansatz, each factor in the kinetic-energy part of the Green's function, Eq. (6), simplifies to

$$\langle \boldsymbol{r}'| \exp(\tau \nabla^2/2)|\boldsymbol{r}\rangle \approx \langle x', y', z'| \exp(\tau \nabla^2/2)|x, y, z\rangle, \quad (7)$$

$$= \langle x + n_x\delta, y + n_y\delta, z + n_z\delta| \exp(\tau \nabla^2/2)|x, y, z\rangle, \quad (8)$$

$$= p_{n_x} p_{n_y} p_{n_z}, \quad (9)$$

with

$$p_n = \langle x + n\delta| \exp\left(\frac{\tau}{2} \frac{\partial^2}{\partial x^2}\right)|x\rangle, \quad (10)$$

$$= \frac{1}{2\pi} \int_{-\pi}^{\pi} \cos(kn) \exp\left\{-\frac{2\tau}{\delta^2} \sin^2\left(\frac{k}{2}\right)\right\} dk, \quad (11)$$

where it should be understood that (x, y, z) and (x', y', z') are grid points and n_x, n_y, and n_z are integer displacements. For the derivation of Eq. (11), see Appendix A.

Evidently, p_n is the non-Gaussian transition probability of a particle hopping from a grid point to its nth nearest neighbor (where n is a positive or negative integer) in an infinite, evenly spaced, 1D grid. It satisfies the following properties expected of such probability:

$$p_n = \delta_{n0} \text{ for } \tau = 0, \quad (12)$$

$$p_n \geqslant 0, \quad (13)$$

and

$$\sum_{n=-\infty}^{\infty} p_n = 1. \quad (14)$$

The proofs of these identities can be found in Appendix B.

Equation (5) contains moves essentially corresponding to an interchange of particles with the same spin, which should, therefore, reverse its sign when applicable. This can be encoded by introducing a canonical order of the grid points and associating the Green's function with the parity of the permutation that brings the sequence of the destination grid points into a canonical order. In this work, we define a canonical order as one with the increasing x coordinates first, then with the increasing y coordinates, and, finally, with the increasing z coordinates. Examples of sign-preserving and sign-flipping moves are depicted in Fig. 1 for a simple case of two same-spin fermions on a 2D grid. We note that a choice of the ordering scheme does not affect simulation results and is only a matter of convenience.

The foregoing equations admit a stochastic implementation similar to DMC [2,3] with a major difference being in the definition of random walkers and their (signed) transition probabilities. Each walker represents a set of all particles, carrying a unit signed weight, $c = \pm 1$. The ith particle has spatial coordinates that are on a point in an infinite, uniform grid with a grid spacing of δ and spin label $s_i = \pm 1/2$ (in the case of an electron) so that $\sum_{i=1}^{N} s_i = S_z$, where S_z is the total magnetic spin angular momentum quantum number of the target state. The walker weight c flips sign whenever an odd number of permutations is needed to bring the particle coordinates into a canonical order after a move. The calculation workflow is similar to that of DMC and consists of the following steps:

(i) *Initialization.* An initial walker population is randomly generated from some real trial wave function $|\Psi_T(\boldsymbol{r}_1, \ldots, \boldsymbol{r}_N)|$ (which must not be confused with a trial wave function in the fixed-node approximation) by the Metropolis algorithm [24], exercising care to avoid Coulomb singularities. The initial walker weights are assigned with the sign of Ψ_T. Factors p_n of Eq. (11) are computed as a function of n by numerical integration and stored.
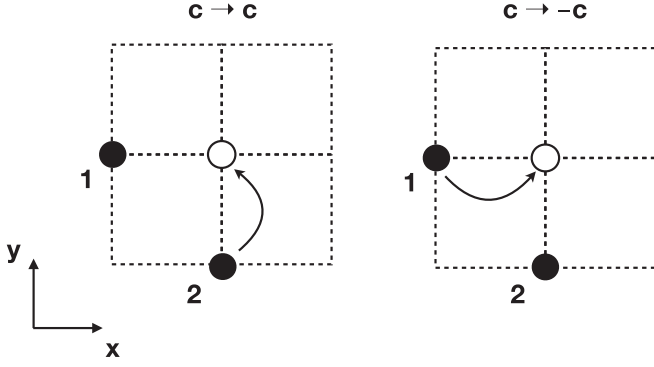
FIG. 1. Examples of sign-preserving (left) and sign-flipping (right) moves for two fermions (labeled "1" and "2") with the same spin on a 2D grid. The grid points are ordered in the increasing x coordinates first and then in the increasing y coordinates so that $r_1 < r_2$ in both cases before the walker moves. In the move shown on the left, the coordinates of particles 1 and 2 are in a canonical order after the move, preserving the sign of c. The move shown on the right brings the coordinates of particles 1 and 2 into a noncanonical order (i.e., $r_1 < r_2$ no longer holds), which needs to be permuted once to be canonical ordered, causing a sign flip in c. In the case of N electrons the new particle coordinates are sorted and the phase is determined from the parity of associated permutation.

(ii) *Propagation.* Each walker performs a random walk. This step is executed by looping over all particles ($i = 1, \ldots, N$) and displacing the grid coordinates of each particle relatively by (n_x, n_y, n_z) with a transition probability of $p_{n_x} p_{n_y} p_{n_z}$. The walker weight $c = \pm 1$ is then multiplied by $(-1)^{[P]}$, where $[P]$ is the parity of permutation P that brings the sequence of the new particle coordinates into a canonical order. $[P]$ is calculated by examining permutations of the like-spin particles separately for $s_i = \pm 1/2$ and, therefore, $[P] = [P_{1/2}] + [P_{-1/2}]$ since $P = P_{1/2} P_{-1/2}$.

(iii) *Branching.* For each walker, the old ($r_1, \ldots, r_N$) and new ($r'_1, \ldots, r'_N$) sets of the particle coordinates are used to calculate the branching factor, $m = \exp[-\tau \{(V(\{r'_i\}) + V(\{r_i\}))/2 - \omega\}]$. The walker is subsequently replaced by $\lfloor m + \xi \rfloor$ copies, where ξ is a random number sampled from a uniform distribution on the interval [0,1] and $\lfloor x \rfloor$ is the greatest integer less than or equal to x.

(iv) *Annihilation.* The list of all walkers is sorted and then searched for the members whose particles occupy the identical set of grid points. An equal number of positively and negatively signed walkers among them are annihilated, leaving only a minimal number of like-signed walkers on each set of grid points.

(v) *Energy estimation.* The energy offset ω is updated as $\omega \to \omega + \tau^{-1} \ln(N_w/N'_w)$ to keep the number of walkers approximately constant, where N_w and N'_w are the sizes of the old and new walker lists, respectively. The mean value of ω in the limit of infinite propagation time T can be used to estimate the ground-state energy,

$$E_{\mathrm{gr}} = \langle \omega \rangle, \tag{15}$$

which is known as the growth estimator [25]. A more desirable measure of energy according to statistical uncertainty considerations is the projection estimator [16,26] defined as

follows:

$$E_{\mathrm{proj}} = \left\langle \frac{\sum_k c_k \hat{H} \Psi_T (r_1^{[k]}, \ldots, r_N^{[k]})}{\sum_k c_k \Psi_T (r_1^{[k]}, \ldots, r_N^{[k]})} \right\rangle \tag{16}$$

as $T \to \infty$, where c_k and $(r_1^{[k]}, \ldots, r_N^{[k]})$ are the weight and grid points of the kth walker, and Ψ_T is any trial wave function (which may differ from the one used in Step 1) having a nonzero overlap with the exact wave function.

Steps 2 through 5 are repeated (with each cycle counted as one Monte Carlo step) until convergence. For a sufficiently large number of walkers, N_w, the computational cost of a Monte Carlo cycle is dominated by the annihilation step, which exhibits $N_w \ln N_w$ scaling of computational complexity owing to the need to sort the walker list. As will be shown in the next section, another important implication of the annihilation is the existence of the critical number of walkers, N_c, required to obtain the correct nodal structure, which grows exponentially with the dimension of the configuration space. The value of N_c determines the memory footprint and limits the application size. The lack of annihilation for a small number of walkers, i.e., $N_w < N_c$, leads to node sampling errors and introduces a nodal bias in the energy estimates [16].

III. RESULTS AND DISCUSSION

A Python program of grid DMC was written and made available online [27]. The transition probabilities p_n were calculated (with a maximum error of 10^{-10}) using the Clenshaw-Curtis adaptive quadrature implemented in the GNU scientific library [28]. Displacements with the probabilities smaller than 10^{-8} were discarded. Statistical errors in the energies were evaluated using the blocking analysis [29] as implemented in PYBLOCK module [30].

A. Fermions in a harmonic trap

Consider a system of four noninteracting spin-1/2 particles with a unit mass confined in a 1D harmonic trap characterized by a potential, $V = \sum_{i=1}^4 x_i^2/2$, where x_i is the ith particle coordinate. It lends itself to analytical solution of the Schrödinger equation with the exact energy, $E = \sum_{i=1}^4 (n_i + 1/2)$ in atomic units (a.u.) or Hartree (E_h), where n_i is the ith quantum number of the 1D harmonic oscillator which is a non-negative integer. States with the total spin quantum number $S = 0$, 1, and 2 were studied by grid DMC with a grid spacing of $\delta = 0.1$ a.u. and an imaginary time step of $\tau = 0.1$ a.u. The initial particle positions were sampled from a uniform distribution on a 6.0-a.u. interval centered at the origin. An ensemble of $\sim 10^7$ random walkers was propagated over 5000 Monte Carlo steps. The energy was evaluated by the growth estimator. Table I compiles the results.

The $S = 0$ ground state has a pair of particles with opposite spins occupying the $n = 0$ one-particle harmonic-oscillator level and another such pair occupying the $n = 1$ level, having the exact energy of $4.0 E_h$. The $S = 1$ ground state has two particles with opposite spins in the $n = 0$ level and one particle with the same spin each in the $n = 1$ and 2 levels, whereas the $S = 2$ ground state has one particle with the same spin each in the $n = 0$, 1, 2, and 3 levels. The correct nodal

TABLE I. Growth-estimator energies (statistical uncertainties in parentheses) in E_h of the $S = 0$, 1, and 2 states of the system with four noninteracting spin-1/2 fermions with a mass of 1 a.u. in a 1D harmonic trap.

S	Grid DMC[a]	Grid[b]	Exact[c]
0	3.99458(4)	3.99625	4.0
1	4.99168(4)	4.99374	5.0
2	7.98292(5)	7.98622	8.0

[a]A grid spacing of 0.1 a.u. and an imaginary time step of 0.1 a.u.
[b]Central three-point finite-difference method with a grid spacing of 0.1 a.u.
[c]Analytical results.

structure of the four-particle wave function naturally emerges in these grid DMC calculations. In DMC with the fixed-node approximation, the wave function in each nodal pocket has the correct shape, but not throughout the whole space even after adjusting the sign of each pocket. In contrast, the wave function obtained in grid DMC has the correct shape in the whole space.

The grid DMC energies are accurate within 0.006, 0.01, and 0.02 E_h of the exact values of the $S = 0$, 1, and 2 states, respectively. They are many orders of magnitude greater than the statistical uncertainty of $\sim 5 \times 10^{-5} E_h$, and so they are biases. The main sources of the biases are the nonzero grid spacing and finite time step. When the deterministic calculations were performed using the same grid (i.e., the diagonalization of the discretized Hamiltonian on a uniform grid spanning 6 a.u. using the central three-point finite-difference formula with $\delta = 0.1$ a.u.), their energies are within 0.002-0.004 E_h of the grid DMC results. These remaining biases are attributed to the finite time step.

In order to study the efficacy of the walker annihilation, we performed a series of runs with varying walker ensemble sizes. The simulation results are given in Fig. 2. The left panel shows that the energies converge at the correct limits, provided that the annihilation events are sufficiently frequent
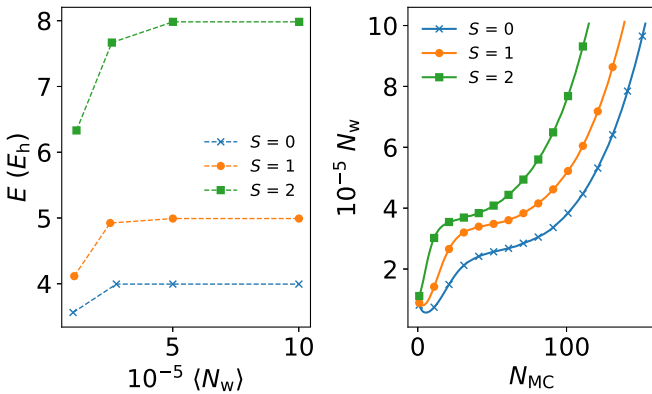

FIG. 2. Left: The energy evaluated by the growth estimator, E, as a function of the average number of walkers, $\langle N_w \rangle$, for the $S = 0$, 1, and 2 ground states of the four noninteracting fermions in a 1D harmonic trap. Right: The number of walkers, N_w, as a function of the Monte Carlo steps, N_{MC}. The energy onset, ω, was held fixed at 4.25, 5.25, and 8.25 E_h for the states with $S = 0$, 1, and 2, respectively.
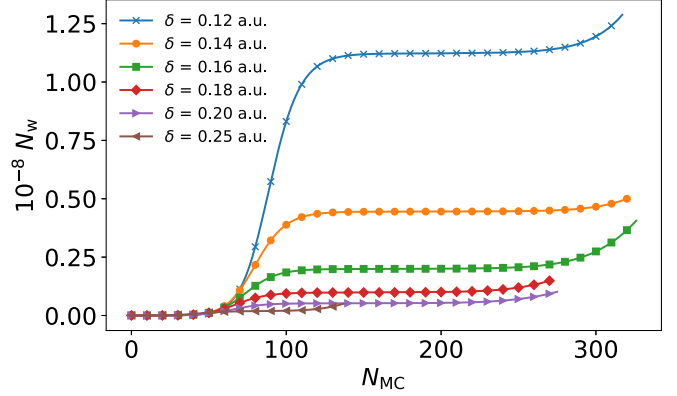

FIG. 3. The number of walkers, N_w, as a function of the Monte Carlo steps, N_{MC}, in grid DMC for two spin-1/2 fermions in a 3D harmonic trap in the triplet ground state for several grid spacings δ. The energy onset was held fixed at $\omega = 4.5 \, E_h$ and imaginary time step $\tau = 0.1$ a.u.

or, equivalently, the number of walkers exceeds a threshold value N_c, which varies with the character of the target state. The lack of a sufficient number of annihilation events causes the underestimation of the energies. The rate of convergence tends to decrease for higher spin states, in which particles occupy one-particle levels with more nodes. The population dynamics presented in the right panel, obtained by holding ω fixed (a production run adjusts ω), is reminiscent of that obtained in FCIQMC [16], similarly exhibiting pronounced plateaus signaling that N_w has reached N_c. The plateaus occur because of the competition between the spawning and walker annihilation [17].

The dependence of N_c on the grid spacing was further analyzed for two spin-1/2 fermions in a 3D harmonic trap in the triplet ground state (Fig. 3). Due to the higher dimension of the configuration space, N_c is orders of magnitude larger than in the 1D system and exhibits a steep growth with decreasing δ. A least-squares fit suggests that $N_c \approx 339 \, \delta^{-5.99}$. In general, one could expect $N_c \propto \delta^{-nd}$, where n is the number of particles and d is the dimension of the one-particle configuration space.

B. The He atom in the ^3S and ^1S states

The grid DMC algorithm for a system with charged particles requires some modifications to avoid the Coulomb singularities. In contrast to continuous DMC, random walks in a discretized space have a nonzero probability of exact particle coalescence, leading to divergent branching factors. To avoid this, we placed the He nucleus at coordinates $(\delta/2, \delta/2, \delta/2)$, where δ is the grid spacing, and furthermore barred the random walks that result in electron-electron coalescence. Various grid spacings δ in the range of 0.01 to 0.16 a.u. were tested, while an imaginary time step of 0.005 a.u. was used in all calculations.

For comparison, we also performed grid DMC calculations for the ^3S state with the fixed-node approximation using the exact nodal structure [31] as well as for the nodeless ^1S ground state [32]. The nodal constraint was imposed by killing walkers attempting to acquire a sign inconsistent with that of a trial

TABLE II. Projection-estimator energies, E (statistical uncertainties in parentheses) of the He atom in the ^3S and ^1S states obtained by grid DMC (with an imaginary time step of 0.005 a.u.) with and without an exact nodal constraint. δ is the grid spacing, $\langle N_w \rangle$ is the average number of walkers, and w is the proportion of walkers having the correct sign.

State	Method	δ / a.u.	$\langle N_w \rangle$	w / %	E / E_h
^3S	Grid DMC	0.16	3.5×10^7	97.9	$-2.12695(1)$
^3S	Grid DMC	0.16	7.0×10^7	98.3	$-2.12687(1)$
^3S	Grid DMC (fn[a])	0.16	10^4	100	$-2.1278(8)$
^3S	Grid DMC	0.08	6.16×10^8	96.7	$-2.16126(1)$
^3S	Grid DMC	0.08	6.25×10^8	96.8	$-2.16169(1)$
^3S	Grid DMC (fn[a])	0.08	10^4	100	$-2.1612(15)$
^3S	Grid DMC (fn[a])	0.04	10^4	100	$-2.1698(8)$
^3S	Grid DMC (fn[a])	0.02	10^4	100	$-2.1724(10)$
^3S	Grid DMC (fn[a])	0.01	10^4	100	$-2.1739(7)$
^3S	Grid DMC (fn[a])	0[b]	10^4	100	-2.1741
^3S	Exact[c]	…	…	…	-2.1753
^1S	Grid DMC	0.16	10^4	100	$-2.8355(22)$
^1S	Grid DMC	0.08	10^4	100	$-2.8867(14)$
^1S	Grid DMC	0.04	10^4	100	$-2.8984(14)$
^1S	Grid DMC	0.02	10^4	100	$-2.9032(16)$
^1S	Grid DMC	0.01	10^4	100	$-2.9029(15)$
^1S	Grid DMC	0[b]	10^4	100	-2.9035
^1S	Exact[c]	…	…	…	-2.9037

[a]Fixed-node approximation using the exact nodal structure.
[b]Extrapolation by a least-squares fitting of the fixed-node results to a quadratic function of δ.
[c]Exact nonrelativistic energies due to Pekeris [33].

wave function Ψ_T having the exact nodal structure. Namely, the walker weight c_k was set to zero if $c_k \Psi_T(\mathbf{r}_1^{[k]}, \mathbf{r}_2^{[k]}) < 0$. With the assistance of the exact nodal structure, grid DMC calculations with the fixed-node approximation need only 10 000 walkers to converge.

The first six rows of Table II list the results of grid DMC calculations with and without the exact nodal constraint using two grid spacings: $\delta = 0.16$ or 0.08 a.u. In both cases, the convergence with respect to the number of walkers was ensured by repeating the calculation with different walker ensemble sizes and checking the stability of the energy estimates. Additionally, the average fraction (w) of walkers with the correct sign (i.e., with the same sign as Ψ_T) was recorded to quantify the accuracy of the nodal structure. The closer the values of w to 100%, the more accurate the nodal structure of the grid DMC result without the fixed-node approximation.

With a coarse grid of $\delta = 0.16$ a.u., convergence is achieved with 3.5 to 7×10^7 walkers (the number identified as N_c) with 97.9 to 98.3% accurate nodal structure. The corresponding energies ($-2.1269 E_h$) have minuscule statistical uncertainties of $10^{-5} E_h$, but suffer from a much greater bias of $1 \text{ m}E_h$ from the one with the exact nodal constraint ($-2.1278 E_h$). This bias is clearly due to an inexact nodal structure and may be called a nodal bias. The grid DMC result with the exact nodal constraint is too high as compared with the exact energy ($-2.1753 E_h$) [33] by $48 \text{ m}E_h$, which must be ascribed to a combination of nonzero grid spacing and finite
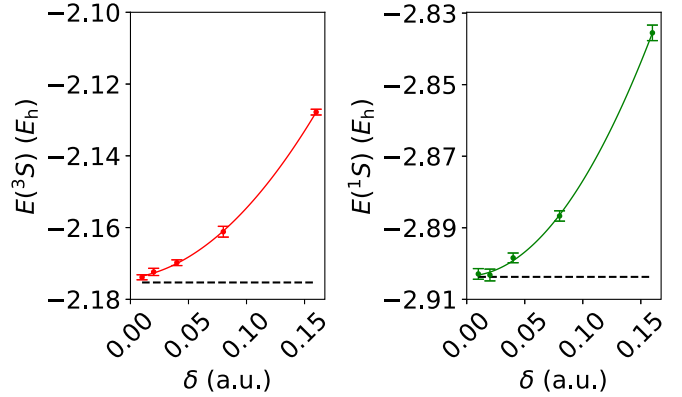

FIG. 4. The energies of the He atom in the ^3S (left) and ^1S (right) states obtained by grid DMC with the exact nodal constraint as a function of the grid spacing (δ). Statistical errors are shown with vertical bars. Horizontal dashed lines indicate the exact nonrelativistic energies [33]. Quadratic fit of the grid-DMC energies are drawn with solid curves.

time step. As will be shown below, a majority of this bias is due to the grid spacing and may be called a grid bias.

Halving the grid spacing to $\delta = 0.08$ a.u. increases N_c by an order of magnitude to 6×10^8. The proportion of walkers with the correct sign deteriorates slightly to 96.7 to 96.8% instead of improves. Interestingly, however, the nodal bias in the energies seems to be compressed to $0.5 \text{ m}E_h$, although this value is obscured by the statistical uncertainty of a similar size in the grid DMC calculation with the exact nodal constraint. Nevertheless, it may be concluded that grid DMC can achieve 97–98% accurate nodal structure *a priori* with a submillihartree nodal bias in the energy for two fermions in the 3D space. Before an extrapolation to $\delta = 0$ limit (see below), it achieves the energy (-2.1613 to $-2.1617 E_h$) of the He atom in the ^3S state within $15 \text{ m}E_h$ of the exact nonrelativisitc value [33] without the Jastrow factor or importance sampling.

Further halving the grid spacing to $\delta = 0.04$ a.u. might elevate the estimated value of N_c to 3.8×10^{10}, approaching a hardware memory limit.

The remainder of the calculations in Table II were performed with the exact nodal constraint for the ^3S and ^1S states with different grid spacings (δ) to estimate a grid bias. Only 10 000 walkers were necessary to converge the energies within a few millihartrees. They are plotted as a function of δ in Fig. 4.

For both states, the plots underscore the slow convergence of the energies to the exact nonrelativistic energies [33]. The slow convergence can be attributed to the inherent inefficiency of a uniform grid in describing electron-nuclear and to a lesser extent electron-electron cusps [19], which may, therefore, be alleviated by the Jastrow or other explicit-correlation factor. Interestingly, the grid acts to suppress the fluctuations in the branching factor by preventing the walkers from closely approaching the nucleus and give rise to the order of magnitude smaller statistical errors as compared to similar continuous DMC calculations [8]. Note that the bias appears to decrease monotonically and seemingly quadratically with δ in the range from 0.16 to 0.01 a.u. For finer grids, the character of convergence is hard to discern as it is masked by

statistical uncertainties. A least-squares fitting of the energies to a quadratic function of δ can extrapolate the energy of each state at $\delta = 0$ that is within $1\,mE_h$ of the respective exact value. This also suggests that the bias is nearly entirely due to a nonzero grid spacing and much less to a finite time step.

IV. SUMMARY AND OUTLOOK

We developed a grid-based quantum Monte Carlo algorithm for a many-fermion wave function with arbitrary nodal structure without invoking the fixed-node approximation. To this end, the original continuous DMC formulation was mapped onto its lattice counterpart by representing the Hamiltonian and corresponding Green's function on an infinite uniform spatial grid using a central finite-difference approximation for the kinetic-energy operator. We showed that the associated propagator is similar to that of the continuous DMC and reduces to it in the limit of zero grid spacing, yet describing a non-Gaussian branching and annihilating random walks of fermions. A key component of the formalism is the definition of a canonical order of particle coordinates, which allows the algorithm to unambiguously encode the antisymmetry of the many-fermion wave function.

Through a few key applications, we demonstrated that our grid DMC algorithm converges at the correct nodal structure *a priori* provided that a total number of walkers exceeds a critical value N_c. The latter determines the memory footprint of the method and restricts its applicability only to low-dimensional problems with smooth potentials. Nevertheless, the correct nodal structure and energy of the He atom in the ^3S state can be determined by this method with accuracy of 97–98% and 99.4%, respectively, without an importance sampling or Jastrow factor. The number of walkers needed for convergence was 10^7 to 10^9, not exceeding 17 GB of memory if 64-bit integers were used to store the walker coordinates on a grid. The remaining bias in the energy seems to be nearly entirely caused by the grid spacing and can be effectively removed by extrapolation [34].

This opens the possibility of realizing practical, scalable, DMC-like stochastic algorithms for two-electron theories, such as MP2 and CCD, which are more widely used in quantum chemistry and solid state physics than exact diagonalization (FCI). A stochastic MP2 algorithm analogous to variational Monte Carlo (VMC) was developed in our group [35] including a Jastrow factor [36], relying on the fact that the MP2 energy is a one-shot evaluation of a high-dimensional integral. It would be desirable to have a stochastic algorithm of more accurate CCD [37], whose energy is no longer a one-shot evaluation, but which requires the determination of two-electron excitation amplitudes having fermion antisymmetry by solving the amplitude equations with an iterative algorithm. We believe that a stochastic route to solving such equations resembles DMC (not VMC) and may be developed on the basis of this work, which should also encompass a DMC-like MP2 algorithm via Sinanoğlu's formulation [21,34].

We note that grid DMC is applicable to an infinite lattice of electrons described by the Hubbard Hamiltonian having the nearest-neighbor hopping and diagonal interaction terms. Only a slight modification of Eq. (11) is needed to account for the periodic boundary conditions. For example, in the case of a one-dimensional Hubbard model [38] with N sites and hopping integral t, Eq. (11) is adjusted to

$$p_n = \frac{1}{N} \sum_{l=0}^{N-1} \cos\left(\frac{2\pi l}{N} n\right) \exp\left[2\tau t \cos\left(\frac{2\pi l}{N}\right)\right]. \quad (17)$$

The detailed analysis of the algorithm's performance for such models is beyond the scope of the present study and will be a subject of future research.

APPENDIX A: DERIVATION OF EQ. (11)

We approximate the second derivative in the kinetic-energy operator by the central three-point finite difference:

$$-\frac{1}{2}\frac{\partial^2}{\partial x^2}\exp(ikx)$$
$$\approx -\frac{1}{2}\frac{\exp[ik(x+\delta)] + \exp[ik(x-\delta)] - 2\exp(ikx)}{\delta^2}$$
$$= -\frac{1}{2}\frac{\exp(ik\delta) + \exp(-ik\delta) - 2}{\delta^2}\exp(ikx)$$
$$= \frac{2}{\delta^2}\sin^2\left(\frac{k\delta}{2}\right)\exp(ikx), \quad (A1)$$

where δ is the grid spacing. The transition probability or Green's function for the kinetic-energy operator on a uniform 1D grid then becomes

$$p_n = \langle x + n\delta| \exp\left(\frac{\tau}{2}\frac{\partial^2}{\partial x^2}\right)|x\rangle$$
$$= \frac{\delta}{2\pi}\int_{-\pi/\delta}^{\pi/\delta} \exp[-ik(x+n\delta)] \exp\left(\frac{\tau}{2}\frac{\partial^2}{\partial x^2}\right)\exp(ikx)\,dk$$
$$\approx \frac{\delta}{2\pi}\int_{-\pi/\delta}^{\pi/\delta} \exp(-ikn\delta) \exp\left[-\frac{2\tau}{\delta^2}\sin^2\left(\frac{k\delta}{2}\right)\right]dk, \quad (A2)$$
$$= \frac{1}{2\pi}\int_{-\pi}^{\pi} \exp(-ik'n) \exp\left[-\frac{2\tau}{\delta^2}\sin^2\left(\frac{k'}{2}\right)\right]dk', \quad (A3)$$

which is identified as Eq. (11). Note that the integration domain $[-\pi/\delta, \pi/\delta]$ is the first Brillouin zone under the periodic boundary condition with lattice constant δ.

The eigenvalue of the discretized kinetic-energy operator reduces to the correct continuous-space limit as $\delta \to 0$:

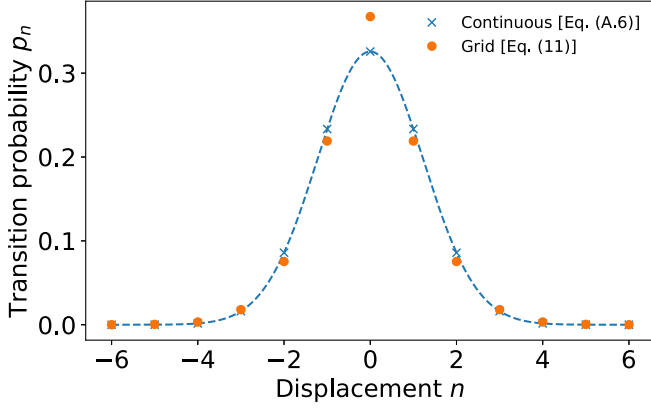$$\lim_{\delta \to 0} \frac{2}{\delta^2}\sin^2\left(\frac{k\delta}{2}\right) = \frac{k^2}{2}. \quad (A4)$$

FIG. 5. Comparison of p_n [Eq. (11) or (A3)] versus Gaussian function [Eq. (A6)] with $\tau = 0.015$ and $\delta = 0.1$.

Expanding the exponent in Eq. (A2) around $\delta = 0$, $\frac{2}{\delta^2} \sin^2(\frac{k\delta}{2}) = \frac{k^2}{2} + o(\delta^2)$, and applying stationary phase arguments to discard higher order terms in δ [39], we find

$$\lim_{\delta \to 0} p_n = \frac{\delta}{2\pi} \int_{-\infty}^{\infty} \exp(-ikn\delta) \exp\left(-\frac{\tau k^2}{2}\right) dk, \quad \text{(A5)}$$

$$= \frac{\delta}{\sqrt{2\pi\tau}} \exp\left(-\frac{n^2\delta^2}{2\tau}\right), \quad \text{(A6)}$$

which is a Gaussian function dictating diffusion in a continuous space. Therefore, taking the limit $\delta \to 0$ in grid DMC, we recover the usual continuous DMC [2,3].

Figure 5 plots the transition probability p_n [Eq. (11) or (A3)] and its $\delta = 0$ limit (a Gaussian function) [Eq. (A6)] as a function of n. The transition probability on a grid differs visibly from the Gaussian function in the $\delta = 0$ limit especially for small n. Specifically, dividing the space into bins slightly increases the probability of staying in the same bin at the expense of decreasing the probability to hop to the nearest or second nearest neighbors. For a greater displacement, the two plots converge because δ becomes small relative to the displacement, making the saddle point approximation asymptotically exact. At every n, p_n is found non-negative.

Equation (11) can, in principle, be generalized for any symmetric finite-difference formula. However, for such a higher-order formula, p_n is usually no longer positive for all n unless $\delta^2 \ll \tau$ (in which case the space is effectively continuous). It is also to be observed that our approach is not immediately extensible to an importance sampling transformation as usually performed in the context of DMC [5] because it breaks the Hermitian and translational symmetry of the kinetic-energy operator by introducing a drift term proportional to the first derivative of the wave function.

APPENDIX B: PROOFS OF EQS. (12)–(14)

A proof of Eq. (12) is trivial.
We have

$$p_n = \frac{1}{2\pi} \int_{-\pi}^{\pi} \cos(kn) \exp\left[-\frac{2\tau}{\delta^2} \sin^2\left(\frac{k}{2}\right)\right] dk$$

$$= \frac{1}{2\pi n} \int_{-\pi n}^{\pi n} \cos(k') \exp\left[-\frac{2\tau}{\delta^2} \sin^2\left(\frac{k'}{2n}\right)\right] dk',$$

where $k' = kn$. It then follows for $n \to \pm\infty$

$$p_n \approx \frac{1}{2\pi|n|} \int_{-\infty}^{\infty} \exp(ik') \exp\left(-\frac{\tau k'^2}{2\delta^2 n^2}\right) dk', \quad \text{(B1)}$$

$$= \frac{\delta}{\sqrt{2\pi\tau}} \exp\left(-\frac{n^2\delta^2}{2\tau}\right) \geqslant 0. \quad \text{(B2)}$$

Equation (B2) implies that p_n and p_{n+1} are non-negative for a sufficiently large $|n|$.

In the meantime, a recursion relationship for p_n can be derived with integration by parts. For $n \neq 0$,

$$p_n = \frac{1}{2\pi} \int_{-\pi}^{\pi} \cos(kn) \exp\left[-\frac{2\tau}{\delta^2} \sin^2\left(\frac{k}{2}\right)\right] dk$$

$$= \frac{1}{2\pi} \left\{ \frac{\sin(kn)}{n} \exp\left[-\frac{2\tau}{\delta^2} \sin^2\left(\frac{k}{2}\right)\right] \right\}_{-\pi}^{\pi}$$

$$+ \frac{1}{2\pi} \int_{-\pi}^{\pi} \frac{\sin(kn)}{n} \frac{\tau \sin(k)}{\delta^2} \exp\left[-\frac{2\tau}{\delta^2} \sin^2\left(\frac{k}{2}\right)\right] dk$$

$$= \frac{\tau}{2\pi n \delta^2} \int_{-\pi}^{\pi} \sin(kn) \sin(k) \exp\left[-\frac{2\tau}{\delta^2} \sin^2\left(\frac{k}{2}\right)\right] dk$$

$$= \frac{\tau}{n\delta^2} \frac{p_{n-1} - p_{n+1}}{2}, \quad \text{(B3)}$$

which can be rearranged to yield

$$p_{n-1} = \frac{2n\delta^2}{\tau} p_n + p_{n+1}. \quad \text{(B4)}$$

This proves Eq. (13) for all n by mathematical induction: Starting from a sufficiently large n that renders both p_n and p_{n+1} non-negative, n is decremented down to zero (vice versa for negative n). The foregoing also implies that p_n is monotonically decreasing with $n \geqslant 0$.

Equation (14) can be proven with the Fourier transform of Dirac's δ function,

$$\sum_{n=-\infty}^{\infty} p_n = \int_{-\pi}^{\pi} \left[\frac{1}{2\pi} \sum_{n=-\infty}^{\infty} \cos(kn) \right] \exp\left[-\frac{2\tau}{\delta^2} \sin^2\left(\frac{k}{2}\right)\right] dk$$

$$= \int_{-\pi}^{\pi} \delta(k) \exp\left[-\frac{2\tau}{\delta^2} \sin^2\left(\frac{k}{2}\right)\right] dk = 1. \quad \text{(B5)}$$

[1] M. H. Kalos, Phys. Rev. **128**, 1791 (1962).

[2] J. B. Anderson, J. Chem. Phys. **63**, 1499 (1975).

[3] A. Lüchow, WIREs Comput. Mol. Sci. **1**, 388 (2011).

[4] D. J. Klein and H. M. Pickett, J. Chem. Phys. **64**, 4811 (1976).

[5] P. J. Reynolds, D. M. Ceperley, B. J. Alder, and W. A. Lester, Jr., J. Chem. Phys. **77**, 5593 (1982).

[6] M. Troyer and U.-J. Wiese, Phys. Rev. Lett. **94**, 170201 (2005).

[7] J. Carlson and M. H. Kalos, Phys. Rev. C **32**, 1735 (1985).

[8] D. F. Coker and R. O. Watts, Mol. Phys. **58**, 1113 (1986).

[9] J. B. Anderson, C. A. Traynor, and B. M. Boghosian, J. Chem. Phys. **95**, 7418 (1991).

[10] M. H. Kalos, Phys. Rev. E **53**, 5420 (1996).

[11] M. H. Kalos and K. E. Schmidt, J. Stat. Phys. **89**, 425 (1997).

[12] M. H. Kalos and F. Pederiva, Phys. Rev. Lett. **85**, 3547 (2000).

[13] Y. Mishchenko, Phys. Rev. E **73**, 026706 (2006).

[14] M. Casula, C. Filippi, and S. Sorella, Phys. Rev. Lett. **95**, 100201 (2005).

[15] M. Casula, S. Moroni, S. Sorella, and C. Filippi, J. Chem. Phys. **132**, 154113 (2010).

[16] G. H. Booth, A. J. W. Thom, and A. Alavi, J. Chem. Phys. **131**, 054106 (2009).

[17] J. S. Spencer, N. S. Blunt, and W. M. C. Foulkes, J. Chem. Phys. **136**, 054110 (2012).

[18] O. Sinanoğlu, J. Chem. Phys. **36**, 3198 (1962).

[19] F. A. Bischoff and E. F. Valeev, J. Chem. Phys. **139**, 114106 (2013).

[20] F. A. Bischoff, R. J. Harrison, and E. F. Valeev, J. Chem. Phys. **137**, 104103 (2012).

[21] S. Hirata, T. Shiozaki, C. M. Johnson, and J. D. Talman, Mol. Phys. **115**, 510 (2017).

[22] J. S. Kottmann and F. A. Bischoff, J. Chem. Theory Comput. **13**, 5945 (2017).

[23] H. F. Trotter, Proc. Am. Math. Soc. **10**, 545 (1959).

[24] N. Metropolis, A. W. Rosenbluth, M. N. Rosenbluth, A. H. Teller, and E. Teller, J. Chem. Phys. **21**, 1087 (1953).

[25] C. J. Umrigar, M. P. Nightingale, and K. J. Runge, J. Chem. Phys. **99**, 2865 (1993).

[26] G. An and J. M. J. van Leeuwen, Phys. Rev. B **44**, 9410 (1991).

[27] A. A. Kunitsa, GRIDDMC: A Python program for grid-based diffusion Monte Carlo (2019), https://github.com/aakunitsa/QMC_grid_theory.git.

[28] M. Galassi, GNU Scientific Library Reference Manual (3rd ed.), http://www.gnu.org/software/gsl/.

[29] H. Flyvbjerg and H. G. Petersen, J. Chem. Phys. **91**, 461 (1989).

[30] J. S. Spencer, PYBLOCK: Python module for performing blocking analysis on data containing serial correlations (2014), https://github.com/jsspencer/pyblock.

[31] D. Bressanini and P. J. Reynolds, Phys. Rev. Lett. **95**, 110201 (2005).

[32] D. M. Ceperley, J. Stat. Phys. **63**, 1237 (1991).

[33] C. L. Pekeris, Phys. Rev. **115**, 1216 (1959).

[34] V. McKoy and N. W. Winter, J. Chem. Phys. **48**, 5514 (1968).

[35] S. Y. Willow, K. S. Kim, and S. Hirata, J. Chem. Phys. **137**, 204122 (2012).

[36] C. M. Johnson, A. E. Doran, J. Zhang, E. F. Valeev, and S. Hirata, J. Chem. Phys. **145**, 154115 (2016).

[37] A. J. W. Thom, Phys. Rev. Lett. **105**, 263004 (2010).

[38] F. H. L. Essler, H. Frahm, F. Göhmann, A. Klümper, and V. E. Korepin, *The One-Dimensional Hubbard Model* (Cambridge University Press, Cambridge, 2005).

[39] J. Mathews and R. L. Walker, *Mathematical Methods of Physics*, 2nd ed. (W. A. Benjamin, New York, 1970).